JASA ARTICLE

Effects of multiaxial pre-stress on Lamb and shear horizontal guided waves

Abdellahi Abderahmane,[1,a)] Alain Lhémery,[1,b)] and Laurent Daniel[2,c)]
[1]*Université Paris-Saclay, CEA-LIST, Gif-sur-Yvette, F-91191, France*
[2]*Université Paris-Saclay, CentraleSupélec, CNRS, Group of Electrical Engineering-Paris (GeePs), Gif-sur-Yvette, F-91192 France*

ABSTRACT:
A theoretical model is derived to extend existing work on the theory of acoustoelasticity in isotropic materials subjected to uniaxial or hydrostatic loadings, up to the case of arbitrary triaxial loading. The model is applied to study guided wave propagation in a plate. The semi-analytical finite element method is adapted to deal with the present theory. Effects of triaxial loading on velocities of Lamb and shear horizontal (SH) modes are studied. They are non-linearly dependent on stress, and this nonlinearity is both frequency-dependent and anisotropic. Velocity changes induced by the effect of stress on the plate thickness are shown to be non-negligible. When a stress is applied, both Lamb and SH modes lose their simple polarization characteristics when they propagate in directions different from the principal directions of stress. The assumption that effects induced by a multiaxial stress equal the sum of effects induced by each of its components independently is tested. Its validity is shown to depend on frequency and propagation direction. Finally, the model is validated by comparing its predictions to theoretical and experimental results of the literature. Its predictions agree very well with measurements and are significantly more accurate than those of existing theories. © *2021 Acoustical Society of America*. https://doi.org/10.1121/10.0003630

(Received 4 November 2020; revised 11 January 2021; accepted 14 February 2021; published online 11 March 2021)
[Editor: Lixi Huang] Pages: 1724–1736

I. INTRODUCTION

The theory of acoustoelasticity (TAE) aims at predicting the effects of mechanical stress on elastic wave velocities. It is based on the theory of finite elastic deformation. One of the first developments of the TAE was proposed by Hughes and Kelly,[1] who based their work upon Murnaghan's theory[2] on finite deformations of an elastic body. They expressed bulk wave velocities in isotropic materials subjected to hydrostatic or uniaxial stresses. Toupin and Bernstein[3] studied the case of infinitesimal dynamic deformation superimposed on a finite static deformation, extending the work of Hughes and Kelly[1] to materials of arbitrary symmetry. The TAE was used to measure Murnaghan constants for polystyrene, iron, and Pyrex glass[1] and for rocks.[4] It was successfully used to estimate mechanical stress in materials subjected to loads below yield point,[5–8] but failed to do so in materials having undergone plastic deformation. This was studied by Crecraft[9] in the case of a nickel-steel bar subjected to beam loading beyond the yield point, who showed that induced velocity changes were not predicted by the theory. Thompson *et al.*[10] studied the case of an aluminium plate subjected to uniaxial loading beyond the yield point, followed by unloading. They described a nonlinear relationship between velocity changes and applied stress in the plastic regime. This effect could not be predicted by the theory. They also found that velocity changes during loading differ from those during unloading, suggesting that plastic deformation modifies elastic properties. In an attempt to model this effect, Kobayashi[11] added an extra term to account for plastic deformation [see Eq. (124) in Ref. 12]. However, this adjustment failed at predicting experimental results, as shown by Hirao and Pao.[13] The case of residual stress induced by welding was studied by Schneider[14] who showed that the theory requires the knowledge of elastic properties of the base material, the weld seam, and the heat affected zone. Otherwise, the theory would be unable to predict measurements[15]

In the work presented here, the study is restricted to loadings below the yield point and the assumption of homogeneous elastic properties is made.

TAE has been less often applied to guided waves (GW) in plates than to bulk waves but several recent publications provided new insights on GW in stressed plates. Gandhi *et al.*[16] applied the TAE as developed by Pao and Gamer[17] to Lamb waves in plates subjected to biaxial loading, with experimental validation in the uniaxial case. Shi *et al.*[18] showed numerically that acoustoelastic effects (AEE) induced by a biaxial stress can be decomposed into the effects induced by the two principal components of stress. Peddeti and Santhanam[19] used the semi-analytical finite element method (SAFEM) to compute velocity changes of Lamb waves in the direction of the—uniaxial—applied

[a)]Also at: Université Paris-Saclay, CentraleSupélec, CNRS, Group of Electrical Engineering-Paris (GeePs), Gif-sur-Yvette, F-91192 France.
[b)]Electronic mail: alain.lhemery@cea.fr
[c)]Also at: Sorbonne Université, CNRS, Group of Electrical Engineering-Paris (GeePs), Paris, F-75252, France, ORCID: 0000-0001-5016-4589.

https://doi.org/10.1121/10.0003630

stress. The authors also studied the case of a plate with stress gradient in its thickness. Yang *et al.*[20] studied the AEE in guides of arbitrary cross section. Zuo *et al.*[21] studied the effect of biaxial and hydrostatic loadings on Lamb waves.

However, none of these authors[16,18–22] have taken into account the effect of stress on the thickness of the plate. This effect was observed experimentally by Murayama *et al.*,[23] who estimated the uniaxial stress during a tensile test, using the two first symmetrical GW modes, namely, the shear horizontal mode SH0 and the Lamb mode *S*0. They found out that stress estimation using *S*0 velocity changes was less accurate than that using SH0 and attributed this discrepancy to the dispersive nature of *S*0 mode. It is shown in the present work that thickness variations induced by stress cannot be overlooked. Furthermore, we found that in Refs. 16 and 18–22, some of the assumptions made are questionable and must be discussed.

On the basis of this review of literature, our findings on the subject of GW propagation in a stressed plate are organized as follows. In Sec. II A, the works by Toupin and Bernstein[3] and by Norris[24] on the TAE are followed, leading to a general study for the equivalent stiffness tensor of a material of arbitrary symmetry subjected to arbitrary stress. In Sec. II B, the study is restricted to isotropic materials, and the equivalent stiffness tensor is written for triaxial applied stress. In Sec. III, the SAFEM is presented with slight adjustments imposed by the TAE to solve the acoustoelastic wave equation in guides. In Sec. IV, effects of stress on Lamb and SH modes are studied. In Sec. IV A, it is shown that when stress is applied, Lamb and SH modes couple. In Sec. IV B, the effect of stress on plate thickness, thus, on guided wave velocities, is studied. This effect cannot be neglected and must therefore be fully included in the TAE applied to GW. In Sec. IV C, the AEE is shown to be non-linear. This non-linearity is both frequency-dependent and anisotropic. In Sec. IV D, we investigate whether or not AEE induced by a multiaxial stress tensor is equal to the sum of AEE induced by each component of the tensor taken separately. In Sec. V, predictions using the present model (which is referred to as the acoustoelastic model, AEM) are compared to experimental and theoretical results by Gandhi *et al.*[16] and theoretical results by Yang *et al.*[20]

Throughout, Einstein's summation convention on repeated indices is used. Bold notations are used for vectorial and tensorial variables.

II. THEORY

The theoretical development of the TAE presented hereafter is divided into two main subsections. In the first (Sec. II A), we follow works by Toupin and Bernstein[3] and by Norris[24] on the TAE. The stiffness tensor of an elastic material subjected to arbitrary static loading is expressed. The subsection is restricted to the basics of the theory, but more detailed calculations accompanied by a discussion on impact of assumptions, are to be found in the Appendix. In the Sec. II B, the stiffness tensor of a stressed material is explicitly written as a function of Cauchy stress and the elastic properties of the material in the stress-free state. This subsection generalizes results found in Ref. 25.

A. TAE

The development of the TAE starts with the identification of three states of the material. The *natural state* S^N is the state of reference, relative to which velocity changes are measured. It is not necessarily stress-free, provided that the elastic properties are known. Having said that, we take the *natural state* in the present work to be un-stressed, considering, we are interested in studying the effects of stress relative to non-stress. The *initial state* S^I is the state of the material after it has undergone a static elastic deformation from its *natural state*. The *final state* S^f results from the superimposition on the initial state of a dynamic deformation—in what follows, that associated with wave propagation—supposed to be small compared to the static one.

Consider a material point P and a rectangular Cartesian coordinate system $R(\boldsymbol{i}_1, \boldsymbol{i}_2, \boldsymbol{i}_3)$, taken as the stationary frame of reference. Its position in the *natural state* is denoted by $\boldsymbol{\xi}$, in the *initial state* by $\boldsymbol{X}$ and the *final state* by $\boldsymbol{x}$. As the *final state* includes dynamic terms, quantities related to this state are time-dependent. For the sake of compactness, their time-dependency is omitted from their notations. Figure 1 shows the various variables and notations introduced in this section.

Displacements of P from one state to the next are denoted by

$$\boldsymbol{u}^I = \boldsymbol{X} - \boldsymbol{\xi}, \quad \boldsymbol{u}^w = \boldsymbol{x} - \boldsymbol{X}, \quad \boldsymbol{u} = \boldsymbol{x} - \boldsymbol{\xi}. \tag{1}$$

The deformation gradient tensor $\boldsymbol{F}$, the Lagrange strain tensor $\boldsymbol{E}$, the Cauchy stress tensor $\boldsymbol{\sigma}$ and the nominal stress tensor $\boldsymbol{N}$ (i.e., the transpose of the first Piola-Kirchhoff stress tensor) from the *natural* to *final states* are given by

$$\boldsymbol{F} = \frac{\partial \boldsymbol{x}}{\partial \boldsymbol{\xi}}, \quad \boldsymbol{E} = \frac{1}{2}(\boldsymbol{F}^T\boldsymbol{F} - \boldsymbol{I}), \quad \boldsymbol{\sigma} = \frac{\boldsymbol{F}}{J}\frac{\partial W}{\partial \boldsymbol{F}}, \quad \boldsymbol{N} = \frac{\partial W}{\partial \boldsymbol{E}}\boldsymbol{F}^T, \tag{2}$$

where $\boldsymbol{I}$, J, and W denote the identity matrix, the Jacobian determinant, and the elastic deformation energy from the *natural* to *final state*, respectively. W can be written as a Taylor series[3,24] of $\boldsymbol{E}$ as

$$W = \frac{1}{2}C_{ijkl}E_{ij}E_{kl} + \frac{1}{3!}C_{ijklmn}E_{ij}E_{kl}E_{mn}. \tag{3}$$

This expression is referred to as the *constitutive non-linearity*, since by deriving the energy W with respect to the strain $\boldsymbol{E}$, one gets a non-linear constitutive relation. The second non-linearity is referred to as the *geometric non-linearity*, which is represented by the use of the non-linear Lagrange strain tensor $\boldsymbol{E}$ (see the Appendix). These two non-linearities are the sources of the various AEE.

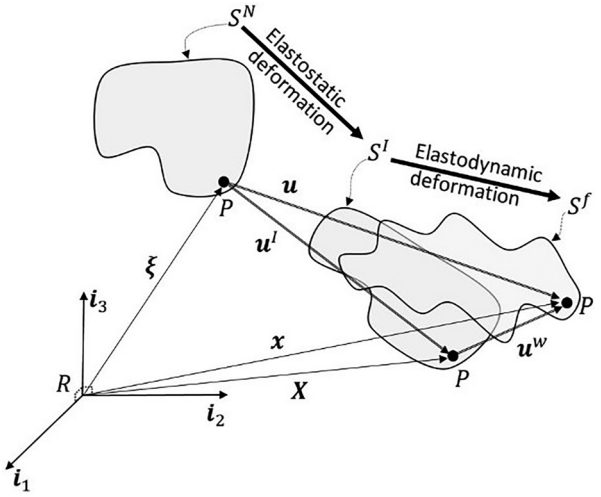

FIG. 1. Schematic representation of variables and notations introduced in the present section.

C_{ijkl} and C_{ijklmn} are the second and third order stiffness tensors in the *natural state*, defined by

$$C_{ijkl} = \left.\frac{\partial W}{\partial E_{ij}\partial E_{kl}}\right|_{\boldsymbol{E}=\boldsymbol{0}}, \quad C_{ijklmn} = \left.\frac{\partial W}{\partial E_{ij}\partial E_{kl}\partial E_{mn}}\right|_{\boldsymbol{E}=\boldsymbol{0}}. \tag{4}$$

Due to the symmetry of $\boldsymbol{E}$ and to the fact that $\partial W/\partial E_{ij}\partial E_{kl} = \partial W/\partial E_{kl}\partial E_{ij}$, the tensor C_{ijkl} possesses the following symmetries:

$$C_{ijkl}=C_{ijlk}=C_{klij}=C_{klji}=C_{lkij}=C_{lkji}=C_{jikl}=C_{jilk}. \tag{5}$$

The equilibrium equation in the *initial state* and the equation of motion in the *final state*, are written as functions of the nominal stress as

$$\nabla_\xi \cdot \boldsymbol{N^I} = 0, \quad \nabla_\xi \cdot N = \rho_0 \frac{\partial^2 \boldsymbol{u}^w}{\partial t^2}, \tag{6}$$

where ρ_0 denotes the density of the material in the *natural state* and $\boldsymbol{N}^I$ denotes the nominal static stress in the *initial state*. Instead of writing the equilibrium equation and the equation of motion using the variables $\boldsymbol{N}$, ρ_0, and $\boldsymbol{\xi}$, the variables $\boldsymbol{\sigma}$, $\rho(\rho = \rho_0/J)$ and $\boldsymbol{x}$ could have been used.[3,26] However, the choice of variables made here allows the use of physical quantities expressed in the *natural stale*, which are supposed to be known.

The equation of motion Eq. (6) is linearized (as detailed in the Appendix) and written as a wave equation in the following form:[24,27]

$$C^{eq}_{abkl}\frac{\partial^2 u^w_k}{\partial X_b \partial X_l} = \rho_0 \frac{\partial^2 u^w_a}{\partial t^2}. \tag{7}$$

In Eq. (7), the equivalent stiffness tensor $\boldsymbol{C}^{eq}$ describes the stiffness of an elastic body of arbitrary symmetry subjected to an arbitrary load. It is decomposed as

$$C^{eq}_{ijkl} = C_{ijkl} + \sum_{q,r,m,n=1}^{3}\left(\left[\delta_{ik}C_{jlqr}\frac{\partial u^I_q}{\partial X_r} + C_{rjkl}\frac{\partial u^I_i}{\partial X_r} + C_{irkl}\frac{\partial u^I_j}{\partial X_r} + C_{ijrl}\frac{\partial u^I_k}{\partial X_r} + C_{ijkr}\frac{\partial u^I_l}{\partial X_r}\right] + \left[C_{ijklmn}\frac{\partial u^I_m}{\partial X_n}\right]\right). \tag{8}$$

The second term (in brackets) originates from the *geometrical nonlinearity* and the third originates from the *constitutive nonlinearity*.

Equation (7) describes the propagation of a wave in a medium subjected to an initial static loading. The solution of this equation, in general (arbitrary symmetry and loading), is impractical for two reasons. First, it involves a large number of parameters for $\boldsymbol{C}^{eq}$(21 for C_{ijkl}, 56 for C_{ijklmn}, and 9 for $u^I_{k,l}$), which in practice are hard if not impossible to know. Second, the expression of $\boldsymbol{C}^{eq}$ does not explicitly use the true stress (Cauchy stress $\boldsymbol{\sigma}$). These two issues are dealt with in the next subsection.

B. Equivalent stiffness C^{eq} as a function of Cauchy stress σ

Expressing the equivalent stiffness $\boldsymbol{C}^{eq}$ as a function of Cauchy stress $\boldsymbol{\sigma}$ is crucial to study the effect of stress on elastic waves. To do that, the method presented here slightly differs from those found in Refs. 16 and 18–22 as we consider debatable some of the assumptions made by their authors. In particular, approximating the Cauchy stress tensor for the second Piola-Kirchhoff tensor [see, for example, Eq. (11) in Ref. 16 or Eq. (34) in Ref. 19], and assuming the latter to be linearly related to the linear part of the strain tensor in the initial state [see, for example, Eq. (13) in Ref. 16 or Eq. (35) in Ref. 19], result in the loss of both the constitutive and the geometric nonlinearities in the initial state. This seems to be inconsistent with the development of the TAE for two reasons. First, the various AEE result from both the constitutive and geometric nonlinearities. Second, in the development of the TAE, elastic deformation from initial to final states (associated with the elastic wave) is supposed to be much smaller than that from natural to initial states. Therefore, if the latter (i.e., the deformation from the natural to the initial states) is treated linearly, then a similar treatment must also be applied to the former (i.e., the deformation from the initial to final states).

Here, the nominal stress tensor is used and no approximation relative to Cauchy stress tensor is made. Furthermore, both the constitutive and the geometric nonlinearities in the initial state are preserved.

The problem at hand is simplified by restricting the study to the case of elastic isotropic materials (in their natural state). In this case, the elastic deformation energy W^I from the natural to initial states is independent of the direction and therefore is only a function of the invariants of Lagrange strain tensor from the natural to the initial states $\boldsymbol{E}^I$. It can be written as[25]

https://doi.org/10.1121/10.0003630

$$W^I = \left(\frac{\lambda+2\mu}{2}\right) I_1^2 - 2\mu I_2 + \frac{n}{3} I_3 + \left(m - \frac{n}{2}\right) I_1 I_2 + \left(\frac{l-m+\frac{n}{2}}{3}\right) I_1^3, \tag{9}$$

where l, m, n denote Murnaghan constants, λ, μ denote Lamé constants, and $I_1 = tr(\boldsymbol{E^I}), I_2 = tr(\boldsymbol{E^{I^2}}), I_3 = tr(\boldsymbol{E^{I^3}})$ denote the invariants of $\boldsymbol{E^I}$.

Upon using the rule of differentiation of the trace of a matrix function by a matrix [i.e., $\partial tr(\boldsymbol{F}(\boldsymbol{X}))/\partial \boldsymbol{X} = \boldsymbol{f}(\boldsymbol{X})^T$, where f is the scalar derivative of F], and substituting Eq. (9) into Eq. (4) yields

$$C_{ijkl} = \lambda\, \delta_{ij}\delta_{kl} + \mu\left(\delta_{ik}\delta_{jl} + \delta_{il}\delta_{jk}\right), \tag{10a}$$

$$C_{ijklmn} = (2l - 2m + n)\delta_{ij}\delta_{kl}\delta_{mn} + (2m - n)\left(\delta_{ij}I_{klmn} + \delta_{kl}I_{mnij} + \delta_{mn}I_{ijkl}\right) + \frac{1}{2}n\left(\delta_{ik}I_{jlmn} + \delta_{il}I_{jkmn} + \delta_{jk}I_{ilmn} + \delta_{jl}I_{ikmn}\right). \tag{10b}$$

where $I_{ijkl} = (1/2)(\delta_{ik}\ \delta_{jl} + \delta_{il}\ \delta_{jk})$. The assumption of isotropy reduced the number of parameters involved in the expressions of C_{ijkl} from 21 to 2 (λ, μ) and of C_{ijklmn} from 56 to 3 (l, m, n). To further reduce the number of parameters in $\boldsymbol{C}^{eq}$, the isotropic material is taken to be subjected to a homogeneous deformation. When it is the case, the position $\boldsymbol{X}$ of the material point P is given as a function of $\boldsymbol{\xi}$ as[26]

$$X_1 = \lambda_1\xi_1, \quad X_2 = \lambda_2\xi_2, \quad X_3 = \lambda_3\xi_3, \tag{11}$$

where $\lambda_1, \lambda_2, \lambda_3$ denote the principal stretches in the principal strain directions, which are chosen (without loss of generality) to coincide with $(\boldsymbol{i}_1, \boldsymbol{i}_2, \boldsymbol{i}_3)$. They are constant since the deformation is homogeneous.

Under these assumptions, $\boldsymbol{C}^{eq}$, $\boldsymbol{E}^I$, $\boldsymbol{F}^I$, and J^I are now written as

$$C^{eq}_{ijkl} = C_{ijkl}\left(\lambda_i + \lambda_j + \lambda_k + \lambda_l - 3\right) + \sum_{q,m=1}^{3}\left(\delta_{ik}C_{jlqq}(\lambda_q - 1) + C_{ijklmm}(\lambda_m - 1)\right), \tag{12a}$$

$$E^I_{ij} = \frac{1}{2}\sum_{k=1}^{3}\left(\frac{\partial X_k}{\partial \xi_i}\frac{\partial X_k}{\partial \xi_j} - \delta_{ij}\right) = \frac{1}{2}\left(\lambda_i^2 - 1\right)\delta_{ij},$$

$$F^I_{ij} = \frac{\partial X_i}{\partial \xi_j} = \lambda_i\delta_{ij}, \quad \text{and} \quad J^I = \lambda_1\lambda_2\lambda_3. \tag{12b}$$

A homogenous deformation takes place in an isotropic material when subjected to triaxial loading $\boldsymbol{\sigma}^I = diag\left(\sigma_1^I, \sigma_2^I, \sigma_3^I\right)$, where σ_i^I are the principal stresses. σ_i^I are in the direction $\boldsymbol{i}_i$ since in isotropic materials, the principal directions of strain coincide with those of stress.

In order to explicitly write $\boldsymbol{C}^{eq}$ as a function of σ_i^I, σ_i^I are written as functions of λ_i. For this, Eqs. (9) and (12b) are substituted into the definition of $\boldsymbol{\sigma}^I$ [i.e., $\boldsymbol{\sigma^I} = (1/J^I)(\boldsymbol{F^I}\partial w^I/\partial \boldsymbol{F^I})$]. One gets

$$\sigma_1^I = \frac{1}{\lambda_2\lambda_3}\left[\lambda_1^5\left(\frac{l}{4} + \frac{m}{2}\right) + \frac{l}{4}(\lambda_1\lambda_2^4 + \lambda_1\lambda_3^4 + 2\lambda_1^3\lambda_2^2 + 2\lambda_1^3\lambda_3^2) + \left(\frac{l}{2} - \frac{m}{2} + \frac{n}{4}\right)\lambda_1\lambda_2^2\lambda_3^2 + \lambda_1^3\left(\frac{\lambda}{2} + \mu - \frac{3l}{2} - m\right) + \left(\frac{\lambda}{2} - \frac{3l}{2} + \frac{m}{2} - \frac{n}{4}\right)\left(\lambda_1\lambda_2^2 + \lambda_1\lambda_3^2\right) - \lambda_1\left(\frac{3\lambda}{2} + \mu - \frac{9l}{4} - \frac{n}{4}\right)\right]. \tag{13}$$

Similar formulas are found for σ_2^I and σ_3^I by simple cyclic permutation of indices 1, 2, and 3.

We now introduce the principal strains E_i defined as $E_i = \lambda_i - 1$. In an isotropic metallic material subjected to loading below yield point, these strains are small compared to 1. This allows approximating $1/\lambda_2\lambda_3$ in the form of a Taylor series by

$$\frac{1}{\lambda_2\lambda_3} \approx 1 - (E_2 + E_3 + E_2E_3) + \left(E_2^2 + E_3^2\right). \tag{14}$$

Replacing λ_i by $1 + E_i$ in Eq. (13), and neglecting terms of orders higher than 2, gives

$$\begin{bmatrix}\sigma_1^I\\ \sigma_2^I\\ \sigma_3^I\end{bmatrix} = \begin{bmatrix}\lambda+2\mu & \lambda & \lambda\\ \lambda & \lambda+2\mu & \lambda\\ \lambda & \lambda & \lambda+2\mu\end{bmatrix}\begin{bmatrix}E_1\\ E_2\\ E_3\end{bmatrix} - \begin{bmatrix}f_1\\ f_2\\ f_3\end{bmatrix}, \tag{15}$$

where

$$f_1 = aE_1^2 + b\left(E_2^2 + E_3^2\right) + c(E_1E_2 + E_1E_3) + dE_2E_3, \tag{16}$$

f_2 and f_3 are found by cyclic permutation of indices 1, 2, and 3, and

$$a = \frac{3\lambda}{2} + 3\mu + l + 2m, \quad b = \frac{3\lambda}{2} + l, \tag{17a}$$

$$c = 2\lambda + 2\mu + 2l, \quad d = 2\lambda + 2l - 2m + n. \tag{17b}$$

Now, E_i are written as functions of σ_i and f_i as

$$E_1 = \frac{\sigma_1^I}{E} - \frac{2\nu}{E}\left(\sigma_2^I + \sigma_3^I\right) + \frac{f_1}{E} - \frac{2\nu}{E}(f_2 + f_3), \tag{18}$$

E_2 and E_3 are found by cyclic permutation of indices 1, 2, and 3 and where Young modulus E and Poisson ratio ν are used instead of λ and μ for the sake of compactness.

Developing now the formulas for f_i as functions of σ_i^I and E_i, and neglecting higher orders terms [i.e., $O\left(E_i^3\right)$] yields

$$E_1 = \frac{\sigma_1^I}{E} - \frac{2\nu}{E}\left(\sigma_2^I + \sigma_3^I\right) + P\sigma_1^{I2} + Q\left(\sigma_2^{I2} + \sigma_3^{I2}\right) + R\left(\sigma_1^I\sigma_2^I + \sigma_1^I\sigma_3^I\right) + S\sigma_2^I\sigma_3^I, \tag{19}$$

E_2 and E_3 are found by cyclic permutation of indices 1, 2, and 3 and where

$$P = ak_1^3 - 2ak_2^3 - 2bk_2^3 - 2ck_2^3 + 2bk_1k_2^2 - 2bk_1^2k_2 + 2ck_1k_2^2 - 2ck_1^2k_2 + 3dk_1k_2^2, \tag{20a}$$

$$Q = bk_1^3 - ak_2^3 - 3bk_2^3 - ck_2^3 - dk_2^3 + ak_1k_2^2 - ak_1^2k_2 + bk_1k_2^2 - bk_1^2k_2 + 4ck_1k_2^2 - ck_1^2k_2 + dk_1k_2^2 - dk_1^2k_2, \tag{20b}$$

$$R = ck_1^3 - 2ak_2^3 - 2bk_2^3 - 4ck_2^3 - 2dk_2^3 + 2ak_1k_2^2 - 2ak_1^2k_2 + 8bk_1k_2^2 - 2bk_1^2k_2 + 5ck_1k_2^2 - 2ck_1^2k_2 - 2dk_1^2k_2 + 2dk_1k_2^2, \tag{20c}$$

$$S = dk_1^3 - 2dk_2^3 + 6ak_1k_2^2 + 4bk_1k_2^2 - 4bk_1^2k_2 + 4ck_1k_2^2 - 4ck_1^2k_2 + 3dk_1k_2^2 - 4bk_2^3 - 4ck_2^3, \tag{20d}$$

and

$$k_1 = \frac{1}{E}, \quad k_2 = \frac{2\nu}{E}. \tag{21}$$

Equations (19a)–(19c) generalize those given in Ref. 25 for the hydrostatic ($\sigma_1^I = \sigma_2^I = \sigma_3^I$) or uniaxial ($\sigma_2^I = \sigma_3^I = 0$) cases. Replacing λ_i by $E_i + 1$ and substituting Eqs. (19) into Eq. (12a), allows writing $\boldsymbol{C}^{eq}$ explicitly as a function of σ_i^I after some algebra. For the sake of clarity, $\boldsymbol{C}^{eq}$ is expressed only as a function of E_i, as a full expression of $\boldsymbol{C}^{eq}(\sigma_i^I)$ is very cumbersome. The final expression writes

$$C_{ijkl}^{eq} = C_{ijkl}(E_i + E_j + E_k + E_l + 1) + \sum_{q,m=1}^{3} \left(\delta_{ik} C_{jlqq} E_q + C_{ijklmm} E_m\right). \tag{22}$$

This expression allows the study of the AEE of arbitrary elastic waves.

III. SAFEM FOR ACOUSTO-ELASTICITY

The wave equation [Eq. (7)] derived in Sec. II is now solved in the specific case of propagation in a plate. Plates being multi-directional guides, a new reference frame R' (see Fig. 2) is introduced associated with the direction of wave propagation, making an angle θ around the $\boldsymbol{i}_3$ axis with $\boldsymbol{i}_1$ [i.e., $R' = (\boldsymbol{i}_1', \boldsymbol{i}_2', \boldsymbol{i}_3' = \boldsymbol{i}_3)$].

The method used to solve equation Eq. (7) is the SAFEM, an efficient method for computing wave modes in guiding structures. It has been validated experimentally, for example, among many others for rails and bars,[28] for plates,[29] and with predictions made by the method of superposition of partial bulk waves (SPBW).[19] The SAFEM was chosen to compute both the various modal displacements and dispersion curves. Thanks to the discretization of the plate thickness, it can further be used straightforwardly to investigate nonuniform stress distributions in the plate thickness (not considered herein).

Here, the SAFEM based on the work by Bartoli *et al.*[30] for GWs in anisotropic plates is written with some adjustments required to take into account the AEE. For compactness, $\boldsymbol{u}^w$ is subsequently denoted by $\boldsymbol{u}$.

First, Eq. (7) is written in the frame R', by rotating $\boldsymbol{C}^{eq}$,

$$C_{ijkl}^{eq}(\theta) = \sum_{m,n,p,q=1}^{3} R_{im} R_{jn} R_{kp} R_{lq} C_{mnpq}^{eq}, \tag{23}$$

where R is given by

$$R = \begin{bmatrix} R_{11} & R_{12} & R_{13} \\ R_{21} & R_{22} & R_{23} \\ R_{31} & R_{32} & R_{33} \end{bmatrix} = \begin{bmatrix} \cos(\theta) & -\sin\theta & 0 \\ \sin(\theta) & \cos(\theta) & 0 \\ 0 & 0 & 1 \end{bmatrix}. \tag{24}$$

Equation (7) is then multiplied by a virtual displacement $\delta\boldsymbol{u}$. In the new frame, one gets

$$C_{ijkl}^{eq}(\theta)\, \delta u_i \frac{\partial^2 u_k}{\partial X_j' \partial X_l'} = \rho_0 \delta u_i \frac{\partial^2 u_i}{\partial t^2}. \tag{25}$$

Integrating over the volume $V(\boldsymbol{\sigma})$ of the material in the initial state, in which surface and its normal are denoted by $S(\boldsymbol{\sigma})$ and $\boldsymbol{n}(\boldsymbol{\sigma})$, and using integration by parts yields

$$\int_{V(\boldsymbol{\sigma})} \frac{\partial \delta u_i}{\partial X_j'} C_{ijkl}^{eq}(\theta) \frac{\partial u_k}{\partial X_l'} dV - \int_{S(\boldsymbol{\sigma})} C_{ijkl}^{eq}(\theta) \delta u_i \frac{\partial u_k}{\partial X_l'} n_l(\boldsymbol{\sigma}) dS = -\int_{V(\boldsymbol{\sigma})} \rho_0 \delta u_i \frac{\partial^2 u_i}{\partial t^2} dV. \tag{26}$$

Dependency on stress is enlightened with the notations $V(\boldsymbol{\sigma})$, $S(\boldsymbol{\sigma})$, and $\boldsymbol{n}(\boldsymbol{\sigma})$ and cannot *a priori* be ignored. We are interested in the effect of static stress on waves in guiding structures whose velocities are fundamentally dependent on the guide section (on the thickness for a plate). To the best of our knowledge, the literature on guided propagation in structures subjected to static stress[16,18–22] does not take into account the effect of stress on the guide section. Here, stresses of the type $\boldsymbol{\sigma}^I = diag(\sigma_1, \sigma_2, \sigma_3)$ are considered, where σ_i are the principal stresses. The normal to the surface is unchanged since the deformation induced by such a stress transforms a cube, making it rectangular parallelepiped. We

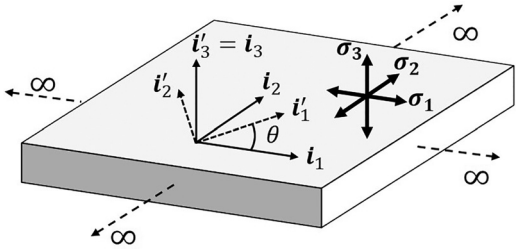

FIG. 2. $R'(\boldsymbol{i}_1', \boldsymbol{i}_2', \boldsymbol{i}_3')$ is the reference frame associated with the wave direction $\boldsymbol{i}_1'$ making an angle $\theta = (\boldsymbol{i}_1, \boldsymbol{i}_1')$ with the initial frame $R(\boldsymbol{i}_1, \boldsymbol{i}_2, \boldsymbol{i}_3)$, in a plate subjected to an arbitrary triaxial stress $\boldsymbol{\sigma} = diag(\sigma_1, \sigma_2, \sigma_3)$.

https://doi.org/10.1121/10.0003630

further assume that the effects of the static stress are fully taken into account through the variations of both the elastic properties and the plate thickness.

The plate surface is considered free [i.e., on S $(\partial u_k/\partial X_l' = 0)$]. For a plate infinite in the plane $(\boldsymbol{i}_1', \boldsymbol{i}_2')$, integration over $V(\boldsymbol{\sigma})$ reduces to an integration over the thickness $d(\boldsymbol{\sigma})$ in the direction $\boldsymbol{i}_3$. Equation (26) simplifies into

$$\int_{d(\boldsymbol{\sigma})} \frac{\partial \delta u_i}{\partial X_j'} C_{ijkl}^{eq}(\theta) \frac{\partial u_k}{\partial X_l'} dX_3 = -\int_{d(\boldsymbol{\sigma})} \rho_0 \delta u_i \frac{\partial^2 u_i}{\partial t^2} dX_3. \quad (27)$$

When a triaxial load is applied, the thickness is expressed by

$$d(\boldsymbol{\sigma}) = d_{\boldsymbol{0}}\,(1 + E_3(\boldsymbol{\sigma})), \quad (28)$$

where d_0 denotes the thickness before the load is applied and E_3 denotes the strain in the direction $\boldsymbol{i}_3$ [see Eq. (19c)]. The SAFEM uses an analytical solution for the propagation in direction $(\boldsymbol{i}_1')$ and a finite element solution in the section. For an infinite plate, the three components of the particle displacement are only functions of X_1' and X_3. For one element of the discretized thickness, they are written as[30]

$$\begin{aligned} \boldsymbol{u_e}\left(X_1', X_3, t\right) &= \begin{bmatrix} u_1(X_3) \\ u_2(X_3) \\ u_3(X_3) \end{bmatrix} e^{i\left(\omega t - kX_1'\right)} \\ &= \boldsymbol{N}(X_3)\boldsymbol{Q_e} e^{i\left(\omega t - kX_1'\right)}, \end{aligned} \quad (29)$$

where ω, t, k denote the angular frequency, the time, and wave number, respectively. $\boldsymbol{N}$ is the matrix of shape functions and $\boldsymbol{Q_e}$ is that of nodal displacements of the element:

$$N = \begin{bmatrix} N^{(1)} & 0 & 0 \\ 0 & N^{(1)} & 0 \\ 0 & 0 & N^{(1)} \\ N^{(2)} & 0 & 0 \\ 0 & N^{(2)} & 0 \\ 0 & 0 & N^{(2)} \\ \vdots & 0 & 0 \\ 0 & \vdots & 0 \\ 0 & 0 & \vdots \\ N^{(n)} & 0 & 0 \\ 0 & N^{(n)} & 0 \\ 0 & 0 & N^{(n)} \end{bmatrix}^T \quad (30)$$

and

$$\boldsymbol{Q_e} = \left[u_1^{(1)}, u_2^{(1)}, u_3^{(1)}, \ldots, u_1^{(n)}, u_2^{(n)}, u_3^{(n)}\right]^T.$$

The notation $[\ \ ]^{(n)}$ refers to the number of nodes per element $(n \geq 2)$. Standard developments of the SAFEM[30,31] dealing with linear elastodynamics use the symmetries of C_{ijkl} recalled by Eq. (5). Voigt notation is used to transform the 4th order stiffness tensor into a 6×6 matrix. Here, acousto-elasticity prevents us from doing so, since the equivalent stiffness tensor $\boldsymbol{C}^{eq}$ does not possess the required symmetries. This is easily shown hereafter. The various terms appearing in Eq. (22) can be sorted into two groups,

$$\begin{aligned} C_{ijkl}^{eq} = &\left[C_{ijkl}(E_i + E_j + E_k + E_l + 1) + \sum_{m=1}^{3} C_{ijklmm} E_m\right] \\ &+ \sum_{q=1}^{3} \delta_{ik} C_{jlqq} E_q. \end{aligned} \quad (31)$$

The two first terms (in square brackets) possess the same symmetries as C_{ijkl} [Eq. (5)]. A simple counterexample proves the third does not. Let us take $i = 1, j = 2, k = 1$ and $l = 2$; one has $\delta_{11} C_{22qq} e_q = \lambda + 2\mu\delta_{2q} \neq \delta_{21} C_{12qq} e_q = 0$; thus, $C_{ijkl}^{eq} \neq C_{jikl}^{eq}$. To apply the SAFEM in the presence of stress by accounting for these lower symmetries, the following notation is used ($11 \rightarrow 1$, $22 \rightarrow 2$, $33 \rightarrow 3$, $23 \rightarrow 4$, $31 \rightarrow 5$, $12 \rightarrow 6$, $32 \rightarrow 7$, $13 \rightarrow 8$, $21 \rightarrow 9$), allowing to rewrite $\boldsymbol{C}^{eq}$ as a 9×9 matrix. Applying the same notation to the gradient of displacement $\partial u_k/\partial X_l'$ leads to

$$\frac{\partial \boldsymbol{u}}{\partial \boldsymbol{X}'} = \boldsymbol{L_1} \frac{\partial}{\partial X_1'} \begin{bmatrix} u_1 \\ u_2 \\ u_3 \end{bmatrix} e^{i\left(\omega t - kX_1'\right)} + \boldsymbol{L_3} \frac{\partial}{\partial X_3} \begin{bmatrix} u_1 \\ u_2 \\ u_3 \end{bmatrix} e^{i\left(\omega t - kX_1'\right)}, \quad (32)$$

where

$$\boldsymbol{L_1} = \begin{bmatrix} 1 & 0 & 0 \\ 0 & 0 & 0 \\ 0 & 0 & 0 \\ 0 & 0 & 0 \\ 0 & 0 & 1 \\ 0 & 0 & 0 \\ 0 & 0 & 0 \\ 0 & 0 & 0 \\ 0 & 1 & 0 \end{bmatrix}, \quad \boldsymbol{L_3} = \begin{bmatrix} 0 & 0 & 0 \\ 0 & 0 & 0 \\ 0 & 0 & 1 \\ 0 & 1 & 0 \\ 0 & 0 & 0 \\ 0 & 0 & 0 \\ 0 & 0 & 0 \\ 1 & 0 & 0 \\ 0 & 0 & 0 \end{bmatrix}. \quad (33)$$

The rest of the development of the method is standard and is found in Refs. 28–30. For one element of the discretized thickness of the plate, one can readily write

$$\left(\boldsymbol{K}_e^{(1)} + ik\boldsymbol{K}_e^{(2)} + k^2\boldsymbol{K}_e^{(3)} - \omega^2\boldsymbol{M_e}\right)\boldsymbol{Q_e} = 0, \quad (34)$$

where elementary stiffness and mass matrices are defined by

$$\begin{aligned} \boldsymbol{K}_e^{(1)} &= \int_{d_e(\sigma)} \boldsymbol{B_1^T} \boldsymbol{C_e^{eq}}(\theta) \boldsymbol{B_1}\, \boldsymbol{d} X_3, \\ \boldsymbol{K}_e^{(2)} &= -\int_{d_e(\sigma)} \left(\boldsymbol{B_1^T} \boldsymbol{C_e^{eq}}(\theta) \boldsymbol{B_2} - \boldsymbol{B_2^T} \boldsymbol{C_e^{eq}}(\theta) \boldsymbol{B_1}\right) \boldsymbol{d} X_3, \quad (35a) \\ \boldsymbol{K}_e^{(3)} &= \int_{d_e(\sigma)} \boldsymbol{B_2^T} \boldsymbol{C_e^{eq}}(\theta) \boldsymbol{B_2}\, \boldsymbol{d} X_3 \text{ and } \boldsymbol{M_e} = \int_{d_e(\sigma)} \boldsymbol{N^T} \rho_e \boldsymbol{N} \boldsymbol{d} X_3, \end{aligned}$$

(35b)

and

$$\boldsymbol{B}_1 = \boldsymbol{L}_3 \cdot \frac{\partial \boldsymbol{N}}{\partial X_3} \quad \text{and} \quad \boldsymbol{B}_2 = \boldsymbol{L}_1 \cdot \boldsymbol{N}. \tag{36}$$

$d_e(\boldsymbol{\sigma})$, $\boldsymbol{C}_e^{eq}$, and ρ_e denote the length, the stiffness, and the density of the element e in the thickness. The global eigenvalue problem is finally obtained by assembling previous elementary matrices,

$$\left(\boldsymbol{K}^{(1)} + ik\boldsymbol{K}^{(2)} + k^2\boldsymbol{K}^{(3)} - \omega^2\boldsymbol{M}\right)\boldsymbol{Q} = \boldsymbol{0}. \tag{37}$$

All but $\boldsymbol{K}^{(2)}$ are symmetric. To overcome this difficulty, Eq. (37) is multiplied on the right by $\boldsymbol{T}^T$ and on the left by $\boldsymbol{T}$, where the matrix $\boldsymbol{T}$ is defined as $\boldsymbol{T} = diag[i, 1, 1, i, 1, 1, \ldots]$. One gets

$$\left(\boldsymbol{K}^{(1)} + k\tilde{\boldsymbol{K}}^{(2)} + k^2\boldsymbol{K}^{(3)} - \omega^2\boldsymbol{M}\right)\tilde{\boldsymbol{Q}} = \boldsymbol{0}, \tag{38}$$

where $\tilde{\boldsymbol{K}}^{(2)} = i\boldsymbol{T}^T\boldsymbol{K}^{(2)}\boldsymbol{T}$ and $\tilde{\mathbf{Q}} = T^T\boldsymbol{Q}$.

At a given frequency (ω), the eigenvalues of the system [Eq. (38)] are the wave numbers of different modes, and the eigenvectors are the particle displacements of these modes. Phase and group velocities at a given frequency write

$$v_p = \frac{\omega}{k} \quad \text{and} \quad v_g = \frac{\tilde{\boldsymbol{Q}}^T\tilde{\boldsymbol{K}}^{(2)}\tilde{\boldsymbol{Q}} + 2k\tilde{\boldsymbol{Q}}^T\boldsymbol{K}^{(3)}\tilde{\boldsymbol{Q}}}{2\omega\tilde{\boldsymbol{Q}}^T\boldsymbol{M}\tilde{\boldsymbol{Q}}}. \tag{39}$$

Their variations in plates under various loadings are studied in the following sections.

IV. NUMERICAL SIMULATIONS

The numerical method described in Sec. III to solve the acoustoelastic wave equation derived in Sec. II is now used to study the effects of static stress on guided modes. The plate considered is 5-mm-thick and made of Al 6061-T6[32] of density equal to 2704 kg.m^{-3} and of elastic properties given by Table I.

Plate thickness is discretized using 10 one-dimensional (1D) three nodes isoparametric elements, a number determined by numerical experiments to ensure accuracy.

Various effects of static stress on wave propagation in plates are studied quantitatively. At first (Sec. IV A), modal particle displacements associated with a mode are shown to differ from those of pure Lamb and SH waves in unstressed isotropic plates and to depend on the wave direction relative to the principal directions of stress. Then (Sec. IV B), the effect of static stress on plate thickness, thus, on the dispersion of guided modes, is studied and shown to be non-negligible compared to other AEE. In Sec. IV C, velocity variations with applied stress are studied. Velocity changes depend non-linearly on stress. This non-linearity is both frequency-dependent and anisotropic. Finally, in Sec. IV D, we test the assumption that the AEE induced in a material by a multiaxial stress (e.g., a triaxial stress) is equal to the sum of the AEE induced by each uniaxial stress taken separately.

A. Acoustoelastic modal displacement

The behavior of GWs in a plate subjected to static stresses differs from that in an unstressed isotropic plate due to the anisotropy induced by stress. Strictly speaking, modes in stressed media cannot anymore be grouped as belonging to families of symmetric or antisymmetric Lamb modes or SH modes, as mentioned by Gandhi[16] and Peddeti and Santhanam[19] but not illustrated numerically.

To be quantitative, the modal components of particle displacement that would be equal to zero in the absence of stress are studied. For a wave-vector aligned on $\boldsymbol{i}_1'$ these components are U_2' for Lamb modes, and U_1' and U_3' for SH modes.

These components are normalized relative to the highest of the maximum amplitudes of U_1' and U_3' for Lamb modes, and to the maximum amplitude of U_2' for SH modes. From now on, one case is treated to exemplify the effects under study. Quantitatively, results being case-dependent, no general rules can strictly be deduced from it. However, many examples have been studied and we can confidently claim that effects exhibited in this subsection are qualitatively typical of those observed in other cases. The plate is subjected to a bi-axial stress ($\sigma_1 = 200$ MPa, $\sigma_2 = -100$ MPa). Note that, because of the symmetries of the loading, Lamb and SH modes propagating along one of the two principal directions of applied stress possess the same symmetries. Therefore, components of these modes that are null in an unstressed medium are still null in these directions of propagation. Modal solutions are computed using the modified SAFEM described in Sec. III, for two directions different from the principal directions of applied stress: $\theta = 30°$, $60°$. A single-frequency excitation of 550 kHz is considered (above the first cut-off frequency of the unstressed guide). Results are shown in Fig. 3.

The components of interest are no longer null and can even be of high amplitude. For example, the in-plane component of $S0$ perpendicular to the propagation direction can be as high as 45% of the component along the propagation direction. Strictly speaking, one should not name modes in stressed media the same name as in unstressed ones. In practice, by following velocity variations in frequency ranges where modes are distinct, it is always possible to label them as being quasi-Lamb modes or quasi-SH modes, if required.

B. Effect of stress on plate thickness thus on GWs

The applied mechanical stress affects velocities through (1) variation of material stiffness, as seen in the expression of $\boldsymbol{C}^{eq}$, (2) variation of material density, which does not appear explicitly in Sec. II, as the dynamic problem is formulated using the nominal stress instead of Cauchy stress,

TABLE I. Al 6061-T6 elastic constants at 25 °C.

Constant	λ	μ	l	m	n
In GPa	56.35	27.5	−281.5	−339	−416

https://doi.org/10.1121/10.0003630

and (3)—this being specific to GWs—variation of the guide section (the thickness for plates). Here, a focus is made on this latter effect, plate thickness variation being described by Eq. (28).

The same plate as in the previous example is considered, this time subjected to in-plane bi-axial tractions ($\sigma_1 = \sigma_2 = 200$ MPa). This loading leads to transversally isotropic elastic properties with respect to the $\boldsymbol{i}_3$ axis, thus, to isotropic propagation of Lamb and SH waves in the $(\boldsymbol{i}_1, \boldsymbol{i}_2)$ plane. This isotropy allows for an easy comparison of velocity changes induced by stress (a tensor), which in general are anisotropic, and those induced by thickness variation (a scalar), which are isotropic.

Let us define three new variables that depict velocity changes, these quantities depending on both the applied stress $\boldsymbol{\sigma}$ and the frequency f. First, Δv_C is the velocity change induced by the effect of stress only on elastic properties (and implicitly on density) given by

$$\Delta v_C = v(\boldsymbol{\sigma}, d_0, f) - v(\mathbf{0}, d_0, f). \tag{40a}$$

Then, Δv_d is the velocity change induced by the effect of stress only on the thickness d of the plate,

$$\Delta v_d = v(\mathbf{0}, d(\boldsymbol{\sigma}), f) - v(\mathbf{0}, d_0, f). \tag{40b}$$

Finally, Δv_T is the total velocity change resulting from the combined effects of stress on elastic properties, density and thickness, written as

$$\Delta v_T = v(\boldsymbol{\sigma}, d(\boldsymbol{\sigma}), f) - v(\mathbf{0}, d_0, f). \tag{40c}$$

Velocity changes of the $S0$ mode as functions of frequency are shown in Fig. 4.

In Fig. 4, the total stress effect on velocity Δv_T (black solid line) is superimposed with the sum of Δv_C and Δv_d (black dots) for both phase and group velocity changes, these two curves almost coincide. This is the first important result that makes it possible to decompose Δv_T into Δv_C and Δv_d.

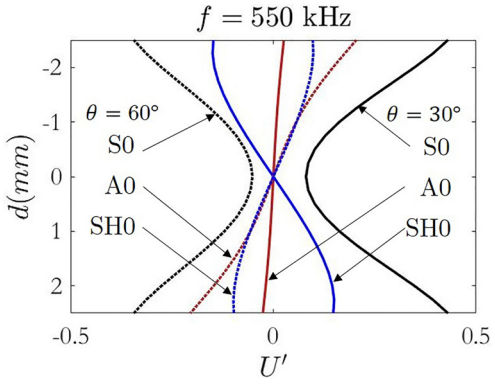

FIG. 3. (Color online) Normalized components of modal particle displacement that would all be equally null in an unstressed medium (see the text for details). $S0$ (black), $A0$ (red), and SH0 (blue) modes at 550 kHz, propagating with an angle of 30° (solid line) 60° (dotted line).

Even more importantly, these results demonstrate that the effect of stress on thickness variation, thus on velocity, cannot be neglected. For example, at 0.56 MHz, phase velocity variation due to stress effects on elasticity is equal to $\Delta v_C \approx 0\,m/s$, while the total variation is equal to $\Delta v_T \approx 5.1\text{m/s} \approx \Delta v_d$. Therefore, if the effect of stress on thickness were neglected, the theory would not account for the phase velocity changes around this frequency. Similarly, at 0.38 MHz, group velocity variation due to elasticity variations equals $\Delta v_C \approx 0\,m/s$ while the total variation equals $\Delta v_T \approx 13.3\text{m/s} \approx \Delta v_d$. One can also notice that Δv_d is higher for $S0$g than for $S0$p, due to its stronger dispersive nature.

Three frequency bands are distinguished, based on the knowledge of the behaviour of $S0$ dispersion. In the middle band $\mathbf{B}_2$, Δv_d is high because $S0$ dispersion is strong in this band. $S0$ dispersion is relatively weak in $\mathbf{B}_1$ and $\mathbf{B}_3$ leading to $\Delta v_d \approx 0\,m/s$ in these frequency bands. Variations of Δv_C are less predictable for example in $\mathbf{B}_1$, $\Delta v_d \approx 0\,m/s$ while Δv_C is large for both phase and group velocities. In $\mathbf{B}_3$ both Δv_d and Δv_C are approximately null. One can conjecture that, in frequency ranges of high velocity dispersion, Δv_C is also high. This has been observed for $A0$, $A1$, SH1, and $S1$ modes, considering the same plate under the same loading. Lack of place prevents us from showing these supplementary results.

C. Nonlinearity of the AEE

It has been shown both theoretically[16,20] and experimentally[16,22,33,34] that stress induced velocity changes for both guided and bulk waves are linearly dependent on the applied stress to a good approximation. Nevertheless, deviations emerge at some frequencies and in some propagation directions for GWs. Let us consider velocity changes of $A1$ propagating in the directions $\theta = 0°$ and 45° at the frequencies $f = 400$ and 500 kHz when the plate is subjected to uniaxial in-plane stress in the range [–200; 200] MPa along $\boldsymbol{i}_1$. Results are given in terms of the relative velocity change $\Delta_r v$ defined as $\Delta_r v = 100 \times \Delta v_T / v(\mathbf{0}, d_0, f)$.

In results at $f = 500$ kHz [Figs. 5(c) and 5(d)], the relationship $\Delta v_r(\boldsymbol{\sigma}) = f(\boldsymbol{\sigma})$ seems linear for both $\theta = 0°$ and $\theta = 45°$. At $f = 400$ kHz, relatively strong nonlinearities appear for $\theta = 45°$. The results of the TAE as presented in Refs. 1, 7, and 17. show that linearity of bulk wave velocity change with stress is only a first order approximation in σ. Present results for GWs show obvious nonlinearities in some of the cases treated. Under a given loading, the relation may be nonlinear and is strongly frequency dependent and anisotropic. In Fig. 5(b), one notices that the behavior in compression ($\sigma_1 < 0$) differs from that in traction ($\sigma_1 > 0$). This is due to $\boldsymbol{C}^{eq}$ and d being quadratic (nonlinear) functions of stress. Equations (19a)–19(c), (28), and (22) show that $d(-\sigma_1) \neq -d(+\sigma_1)$ and $C^{eq}(-\sigma_1) \neq -C^{eq}(+\sigma_1)$. Therefore, $\Delta_r v(-\sigma_1) \neq -\Delta_r v(+\sigma_1)$.

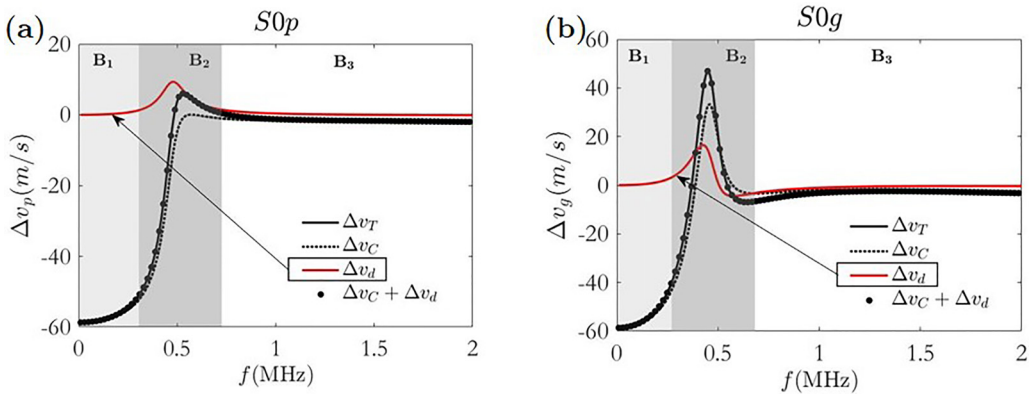

FIG. 4. (Color online) $S0$ velocity changes [phase (a), and group (b)] in a plate subjected to $\sigma_1 = \sigma_2 = 200$ MPa, as functions of the frequency.

Again, these results qualitatively exemplify phenomena observed in other cases but quantitative conclusions cannot be given since they are strongly case-dependent.

D. Decomposition of the AEE

The formalism developed herein can deal with guided modes propagating in isotropic materials subjected to triaxial loading. Here, as in the previous paragraphs, one example is studied to exemplify typical effects observed in the triaxial case. The same plate as in previous examples is now subjected to triaxial loading $\sigma_1 = 100$ MPa, $\sigma_2 = -50$ MPa, and $\sigma_3 = 80$ MPa.

Specifically, effects induced by such a complex loading are compared to the sum of the effects induced by the three uniaxial loadings considered separately. The aim is to study to what extent the assumption of equality can be made.

Mathematically, assuming equal effects induced by the two cases amounts to saying that the total effect of a triaxial stress on velocity changes given by a three-variable function $\Delta v_\sigma = \Delta v(\sigma_1, \sigma_2, \sigma_3)$ can be approximated by terms of its Taylor series that only involve one independent uniaxial loading at a time (terms involving combinations of two of them or three of them are simply ignored in this approximation).

In what follows, the assumption is tested for the $S0$ mode, at four frequencies (0.2, 0.3, 0.5, and 0.6 MHz). Results are shown in Fig. 6 in terms of relative velocity changes. For compactness, relative velocity changes due to the multiaxial stress tensor are denoted by $\Delta_r v_\sigma$ and those due to each component σ_i are denoted by $\Delta_r v_{\sigma_i}$.

In the case of relative phase velocity changes, at all four frequencies, the total relative velocity change due to triaxial loading $\Delta_r v_\sigma$ and the sum of effects due to the three uniaxial loadings $\sum \Delta_r v_{\sigma_i}$ almost superimpose, with very small deviations at $f = 0.5$ MHz. A similar observation is made for the group velocity at the two lower frequencies of 0.2 and 0.3 MHz. At the two higher frequencies (0.5 and 0.6 MHz), $\Delta_r v_\sigma$ and $\sum \Delta_r v_{\sigma_i}$ depart from each other. This leads us to conclude that the validity of the assumption depends on the frequency and on the direction and is not a general rule.

The assumption of equal effects would be a starting point for the development of methods for stress characterization based on velocity changes. But case-dependent parametric study is required to safely use whatever characterization method that would be based on this assumption.

Incidentally, present results evidence the anisotropy of guided wave propagation in stressed media. This is very well-known and was already described for Lamb waves,[16] but also for SH0,[35] Rayleigh and skimming longitudinal waves[14] and bulk waves.[4]

V. COMPARISON WITH EXPERIMENTAL AND THEORETICAL RESULTS OF THE LITERATURE

Experimental and theoretical results published by Gandhi *et al.*[16] and theoretical results by Yang *et al.*[20] are now used for validation purposes of the AEM derived in the present paper. In experiments presented in Ref. 16, an aluminium plate of thickness $d_0 = 6.35$ mm is subjected to a uniaxial in-plane stress. Three modes are studied: $S0$ at 250 kHz, $A1$ at 400 kHz, and $S1$ at 600 kHz. Two sets of measurements were considered. In the first set, phase velocity changes of wave propagation in the direction of a uniaxial loading were measured as functions of the applied stress. The stress is varied from 0 to 57.5 MPa by step of 5.75 MPa. In the second set, phase velocity changes were measured in different directions relative to that of the uniaxial applied stress (the direction 0° being perpendicular to the direction of the applied stress of constant value 57.5 MPa).

As far as predictions made using the present model are concerned, two calculations are made for reproducing the experimental results. In the first, the total effect of stress on wave velocity changes is computed. In the second, the effect of stress on plate thickness is not taken into account. The various results are superimposed on Fig. 7 for an easy quantitative comparison.

Results shown in the left (resp., right) column of Fig. 7 compares phase velocity changes for the first (resp., second) set of measurements and predictions. Predictions made using the present AEM are always in better agreement with measurements than other theoretical predictions. Taking into account the effects induced by thickness variations improves the present predictions (solid lines correspond to predictions made when all the AEEs are taken into account while dashed lines correspond to predictions without

https://doi.org/10.1121/10.0003630

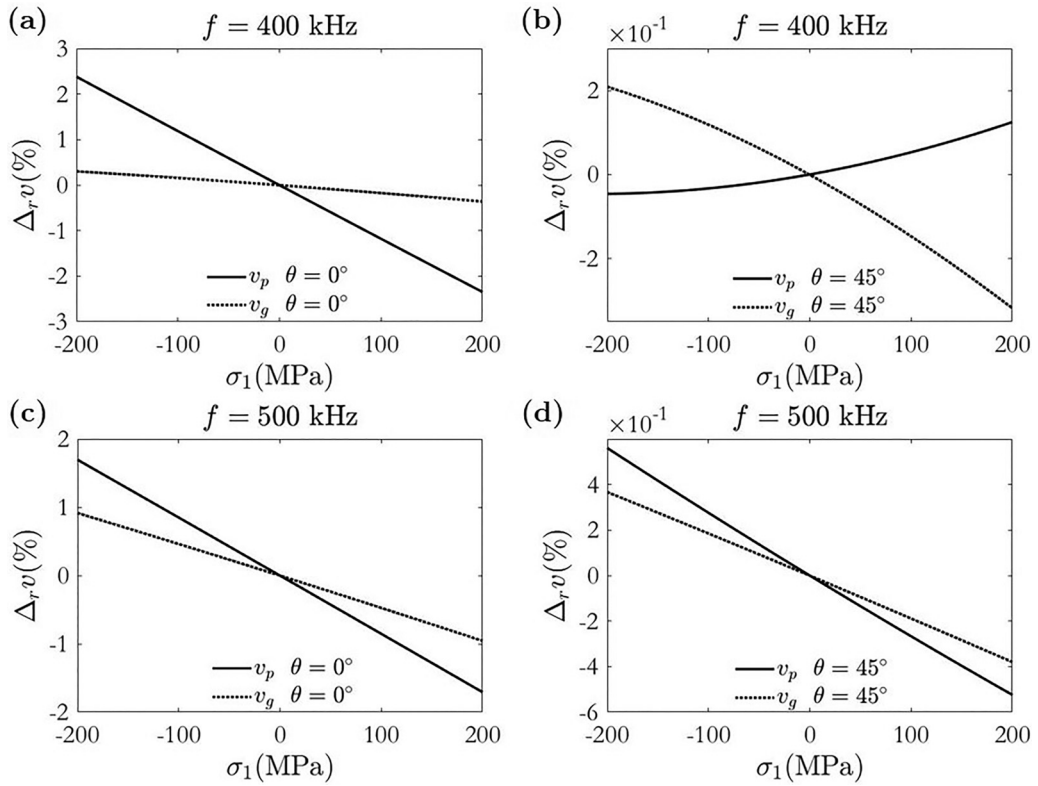

FIG. 5. $A1$ relative velocity changes (phase: solid line, group: dotted line) as functions of uniaxial stress applied in direction $\theta = 0°$. Left column, propagation at an angle $\theta = 0°$. Right column, $\theta = 45°$.

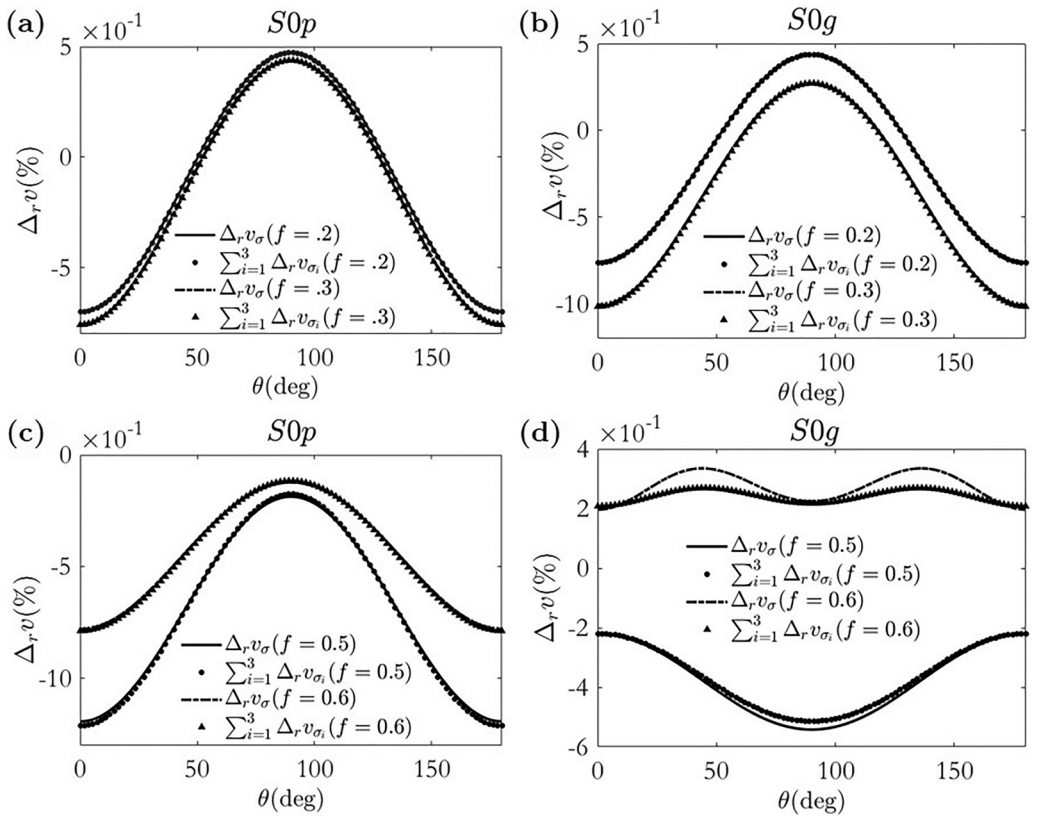

FIG. 6. $S0$ relative velocity changes at four different frequencies. Left column, phase velocity; right column, group velocity (frequencies f in MHz).

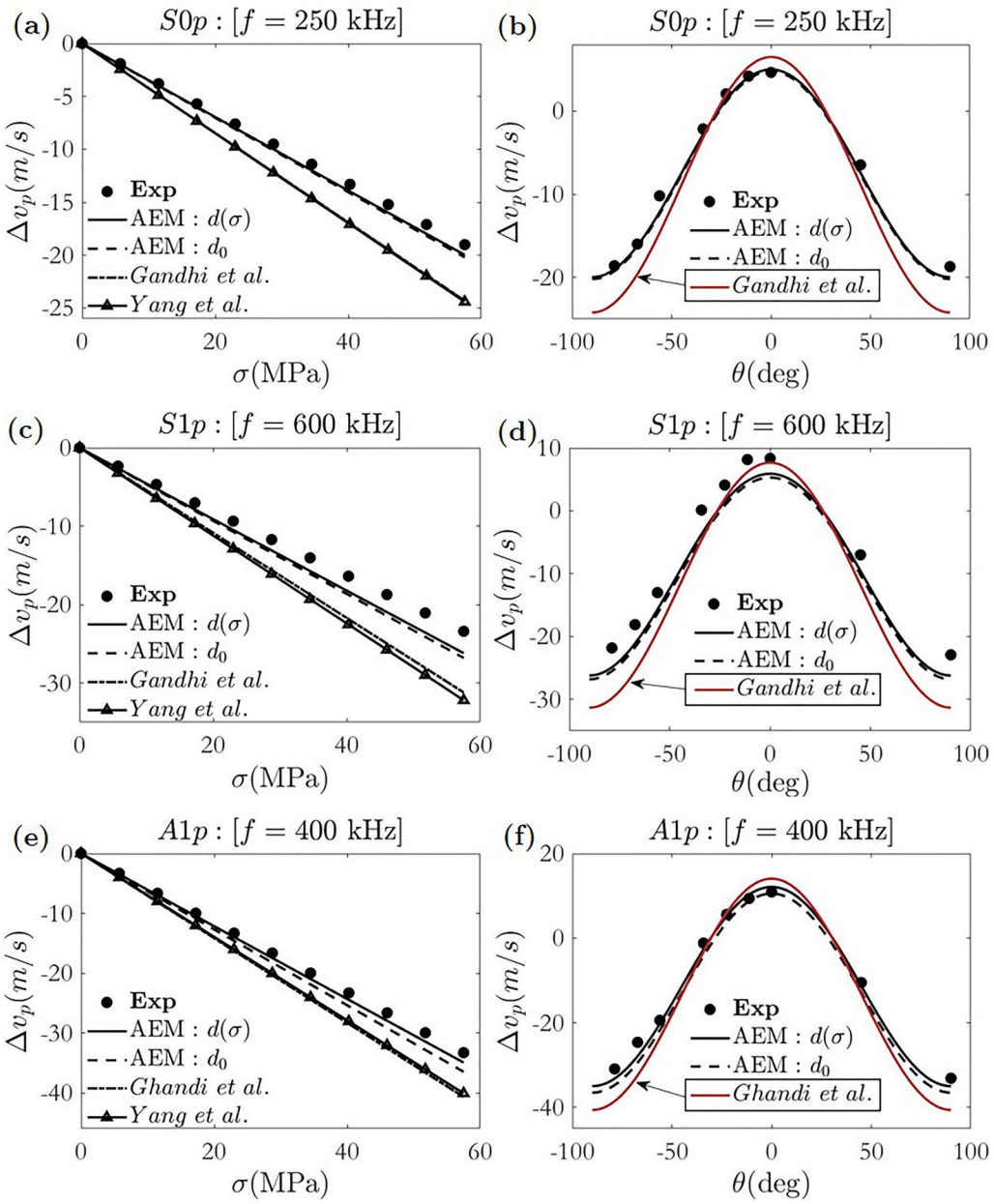

FIG. 7. (Color online) Comparison of measurements by Gandhi *et al*., Ref. 16 theoretical predictions by Gandhi *et al*. Ref. 16 and by Yang *et al*. Ref. 20 (when available), and predictions by the present model (AEM) with account of thickness variations (black solid line) or without (black dashed line).

account of effects induced by thickness variations). This specific effect induced by thickness variations in the case at hand is not as high as what was observed in Sec. IV B (Fig. 4). This is easily explained by the fact that at the frequencies considered in experiments (i.e., $S0$ at 0.25 MHz, $A1$ at 0.4 MHz, and $S1$ at 0.6 MHz), modes involved are only weakly dispersive, leading to small Δv_d.

More importantly, the significant improvement gained using the model derived in the present paper compared to existing models is straightforwardly explained by the fact that terms neglected in previously published models are taken into account here and are really part of the solution (see Sec. II B for a more detailed explanation).

VI. CONCLUSION

In this work, the TAE as described by Toupin and Bernstein[3] then by Norris[24] is used to address the problem of guided wave propagation in plates subjected to multiaxial stresses. The TAE expresses the equivalent stiffness tensor of a material of arbitrary symmetry subjected to arbitrary stresses.

Here, this equivalent stiffness tensor was explicitly written as a function of the applied stress by restricting the present study to the case of isotropic materials. On this basis, formulas derived by Abiza *et al*.[25] for uni-axial or hydrostatic loads were extended up to the case of an arbitrary triaxial loading.

https://doi.org/10.1121/10.0003630

Then, the explicit stiffness tensor was used to study AEEs on guided wave propagation in isotropic plates. It was integrated into the semi-analytical finite element method—which was slightly adjusted—to compute modal solution in plates subjected to static stress. This allowed us to study various effects of stress on GW and to draw a few conclusions. (1) Particle modal displacements of Lamb and SH waves in a stressed plate differ from those in a stress-free one. (2) Stress-induced variations of plate thickness, and consequently of guided wave velocities, were proven to be significant whenever modal dispersion arises (thus, null for the nondispersive mode SH0). (3) Stress-induced velocity changes vary non-linearly with stress, depend on the frequency, and are anisotropic. (4) The AEEs resulting from triaxial loading possibly differ from the sum of effects resulting from each uniaxial loading.

Finally, measurements[16] and predictions[16,20] of the literature were compared to predictions computed with the present AEM. These latter predictions were shown to be quantitatively in better agreement with measurements than existing approximate theories.

APPENDIX: LINEARIZATION OF THE EQUATION OF MOTION

A detailed calculation is proposed, following Ref. 27 with additional assumptions, allowing the equation of motion given by Eq. (6) to be linearized and written as the wave equation given by Eq. (7).

First, $\nabla_\xi \cdot \boldsymbol{N}$ is written as a function of the wave displacement $\boldsymbol{u}^w$ and some quantities from the *initial* and *natural states*. For this, $\boldsymbol{F}$ and $\boldsymbol{E}$ are expressed in terms of the displacement gradient as

$$F_{pb} = \frac{\partial u_p}{\partial \xi_b} + \delta_{pb}, \quad E_{ij} = \frac{1}{2}\left(\frac{\partial u_i}{\partial \xi_j} + \frac{\partial u_j}{\partial \xi_i} + \frac{\partial u_\alpha}{\partial \xi_i}\frac{\partial u_\alpha}{\partial \xi_j}\right). \tag{A1}$$

One can see that $\boldsymbol{E} = \boldsymbol{f}\left(\partial u_i/\partial \xi_j\right)$ is non-linear, this non-linearity being referred to as the *geometric non-linearity*.

Second, we derive the elastic deformation energy W with respect to $\boldsymbol{E}$, which yields

$$\frac{\partial W}{\partial E_{ap}} = \sum_{k,l,m,n=1}^{3}\left(C_{apkl}E_{kl} + \frac{1}{2}C_{apklmn}E_{kl}E_{mn}\right). \tag{A2}$$

By substituting Eq. (A1) and Eq. (A2) into the definition of $\boldsymbol{N}$ in Eq. (2), we find

$$\begin{aligned} N_{ab} = {} & \frac{1}{2}C_{abkl}\left(\frac{\partial u_k}{\partial \xi_l} + \frac{\partial u_l}{\partial \xi_k}\right) + \frac{1}{2}C_{abkl}\frac{\partial u_\alpha}{\partial \xi_k}\frac{\partial u_\alpha}{\partial \xi_l} \\ & + \frac{1}{2}C_{apkl}\left(\frac{\partial u_k}{\partial \xi_l}\frac{\partial u_p}{\partial \xi_b} + \frac{\partial u_l}{\partial \xi_k}\frac{\partial u_p}{\partial \xi_b}\right) \\ & \times \frac{1}{8}C_{abklmn}\left(\frac{\partial u_k}{\partial \xi_l}\frac{\partial u_m}{\partial \xi_n} + \frac{\partial u_k}{\partial \xi_l}\frac{\partial u_n}{\partial \xi_m} + \frac{\partial u_l}{\partial \xi_k}\frac{\partial u_m}{\partial \xi_n}\right. \\ & \left. + \frac{\partial u_l}{\partial \xi_k}\frac{\partial u_n}{\partial \xi_m} + \frac{\partial u_\alpha}{\partial \xi_k}\frac{\partial u_\alpha}{\partial \xi_l}\right) + O\left(\left(\frac{\partial u}{\partial \xi}\right)^3\right). \end{aligned} \tag{A3}$$

We now assume that the higher order terms (>2) of the displacement gradient can be neglected. This assumption is particularly justified for metallic materials subjected to loads below yield point. After rearranging terms in Eq. (A3), one gets

$$N_{ab} = \sum_{k,l,m,n=1}^{3}\left(C_{abkl}\frac{\partial u_k}{\partial \xi_l} + \frac{1}{2}M_{baklmn}\frac{\partial u_k}{\partial \xi_l}\frac{\partial u_m}{\partial \xi_n}\right), \tag{A4}$$

where M is given by

$$M_{abklmn} = C_{abklmn} + C_{abln}\delta_{km} + C_{bnkl}\delta_{am} + C_{blmn}\delta_{ak}. \tag{A5}$$

Nominal stress being expressed in terms of the displacement gradient, ∇_ξ is re-written as a function of the initial displacement $\boldsymbol{u^I}$ and of the initial position $\boldsymbol{X}$, using the chain rule. Formally, one gets

$$\begin{aligned} \frac{\partial}{\partial \xi_i} &= \frac{\partial}{\partial X_r}\frac{\partial X_r}{\partial \xi_i} = \frac{\partial}{\partial X_r}\frac{\partial\left(u_r^I + \xi_r\right)}{\partial \xi_i} \\ &= \frac{\partial}{\partial X_i} + \frac{\partial}{\partial X_r}\frac{\partial u_r^I}{\partial \xi_i} = \frac{\partial}{\partial X_i} + \frac{\partial}{\partial X_r}\cdot\left(\frac{\partial}{\partial X_i} + \frac{\partial}{\partial X_r}\frac{\partial u_r^I}{\partial \xi_i}\right)u_r^I \\ &= \frac{\partial}{\partial X_i} + \frac{\partial u_r^I}{\partial X_i}\frac{\partial}{\partial X_r} + \frac{\partial u_r^I}{\partial X_r}\frac{\partial u_r^I}{\partial \xi_i}\frac{\partial}{\partial X_r}. \end{aligned} \tag{A6}$$

By neglecting the higher terms in $\partial u^I/\partial X$, Eq. (A6) simplifies into

$$\frac{\partial}{\partial \xi_i} = \frac{\partial}{\partial X_i} + \frac{\partial u_r^I}{\partial X_i}\frac{\partial}{\partial X_r}. \tag{A7}$$

Substituting Eq. (A7) into Eq. (A4) and assuming C_{abkl} and M_{baklmn} to be homogenous yields

$$\begin{aligned} \frac{\partial N_{ab}}{\partial \xi_b} = {} & C_{abkl}\left(\frac{\partial^2 u_k}{\partial X_b \partial X_l} + \frac{\partial^2 u_r^I}{\partial X_b \partial X_l}\frac{\partial u_k}{\partial X_r} + \frac{\partial^2 u_k}{\partial X_b \partial X_r}\frac{\partial u_r^I}{\partial X_l}\right) \\ & + \frac{\partial u_r^I}{\partial X_b}C_{abkl}\left(\frac{\partial^2 u_k}{\partial X_r \partial X_l} + \frac{\partial^2 u_r^I}{\partial X_r \partial X_l}\frac{\partial u_k}{\partial X_r} + \frac{\partial^2 u_k}{\partial X_r \partial X_s}\frac{\partial u_s^I}{\partial X_l}\right) \\ & + \frac{1}{2}M_{baklmn}\left(\frac{\partial}{\partial X_b} + \frac{\partial u_r^I}{\partial X_b}\frac{\partial}{\partial X_r}\right) \\ & \times \left(\frac{\partial u_k}{\partial X_l}\frac{\partial u_m}{\partial X_n} + \frac{\partial u_p^I}{\partial X_n}\frac{\partial u_k}{\partial X_l}\frac{\partial u_m}{\partial X_p} + \frac{\partial u_s^I}{\partial X_l}\frac{\partial u_k}{\partial X_s}\frac{\partial u_m}{\partial X_n}\right. \\ & \left. + \frac{\partial u_s^I}{\partial X_l}\frac{\partial u_p^I}{\partial X_n}\frac{\partial u_k}{\partial X_s}\frac{\partial u_m}{\partial X_p}\right). \end{aligned} \tag{A8}$$

Now, $\partial N_{ab}/\partial \xi_b$ is explicitly written as a function of the wave displacement $\boldsymbol{u}^w$ and of quantities taken in the initial and natural states (i.e., C and M). We substitute $\boldsymbol{u}$ by $\boldsymbol{u^I} + \boldsymbol{u^w}$ in the expression of $\partial N_{ab}/\partial \xi_b$. Four terms emerge. The first is static and is null as $\nabla_\xi \cdot \boldsymbol{N^I} = 0$. The second is a function of the product $u_{k,l}^I \cdot u_{m,n}^w$ ($[]_{k,l} = \partial[]_k/\partial X_l$). The third is a function only of $\boldsymbol{u}^w$ and can be neglected under the assumption that the dynamic deformation is far smaller than the

static one. The fourth contains higher order terms in $u^I_{k,l}$ or $u^w_{k,l}$, which can be neglected compared to $u^I_{k,l} \cdot u^w_{m,n}$. This is justified since we are interested in static deformation of metallic materials below yield point.

Finally, the equation of motion reduces to the following wave equation, given by

$$\nabla_\xi \cdot N = \rho_0 \frac{\partial^2 \boldsymbol{u}^w}{\partial t^2} \Rightarrow C^{eq}_{abkl} \frac{\partial^2 u^w_k}{\partial X_b \partial X_l} = \rho_0 \frac{\partial^2 u^w_a}{\partial t^2}. \quad \text{(A9)}$$

[1]D. S. Hughes and J. L. Kelly, "Second order elastic deformation of solids," Phys. Rev. **92**, 1145–1149 (1953).
[2]F. D. Murnaghan, "Finite deformations of an elastic solid," Am. J. Math. **59**, 235–260 (1937).
[3]R. A. Toupin and B. Bernstein, "Sound waves in deformed perfectly elastic materials. Acoustoelastic effect," J. Acoust. Soc. Am. **33**, 216–225 (1961).
[4]P. A. Johnson and P. N. J. Rasolofosaon, "Nonlinear elasticity and stress-induced anisotropy in rock," J. Geophys. Res. B: Solid Earth **101**, 3113–3124, https://doi.org/10.1029/95JB02880 (1996).
[5]D. Vangi, "Stress evaluation by pulse-echo ultrasonic longitudinal wave," Exp. Mech. **41**, 277–281 (2001).
[6]N. N. Hsu, "Acoustical birefringence and the use of ultrasonic waves for experimental stress analysis," Exp. Mech. **14**, 169–176 (1974).
[7]R. B. King and C. M. Fortunko, "Determination of in-plane residual stress states in plates using horizontally polarized shear waves," J. Appl. Phys. **54**, 3027–3035 (1983).
[8]A. V. Clark, Jr. and J. C. Moulder, "Residual stress determination in aluminium using electromagnetic acoustic transducers," Ultrasonics **23**, 253–259 (1985).
[9]D. I. Crecraft, "The measurement of applied and residual stresses in metals using ultrasonic waves," J. Sound Vib. **5**, 173–192 (1967).
[10]R. B. Thompson, J. F. Smith, and S. S. Lee, "Microstructure-independent acoustoelastic measurement of stress," Appl. Phys. Lett. **44**, 296–298 (1984).
[11]M. Kobayashi, "Acoustic theory for plastically deformed solids," Jpn. Soc. Mech. Eng. **48**(432), 1072–1081 (1982) (in Japanese).
[12]Y. H. Pao, W. Sachse, and, and H. Fukuoka, "Acoustoelasticity and ultrasonic measurements of residual stresses," in *Physical Acoustics Vol. XVII*, edited by W. P Mason and R. N Thurston (Academic Press, New York, 1984), Chap. 2, pp. 62–140.
[13]M. Hirao and Y. H. Pao, "Dependence of acoustoelastic birefringence on plastic strains in a beam," J. Acoust. Soc. Am. **77**, 1659–1664 (1985).
[14]E. Schneider, "Ultrasonic techniques," in *Structural and Residual Stress Analysis by Nondestructive Methods*, edited by V. Hauk (Elsevier, Amsterdam, 1977), pp. 522–563.
[15]E. Tanala, G. Bourse, M. Fremiot, and J.-F. de Belleval, "Determination of near surface residual stresses on welded joints using ultrasonic methods," NDT E Int. **28**, 83–88 (1995).
[16]N. Gandhi, J. E. Michaels, and S. J. Lee, "Acoustoelastic Lamb wave propagation in biaxially stressed plates," J. Acoust. Soc. Am. **132**, 1284–1293 (2012).
[17]Y.-H. Pao and U. Gamer, "Acoustoelastic waves in orthotropic media," J. Acoust. Soc. Am. **77**, 806–812 (1985).
[18]F. Shi, J. E. Michaels, and S. J. Lee, "In situ estimation of applied biaxial loads with Lamb waves," J. Acoust. Soc. Am. **133**, 677–687 (2013).
[19]K. Peddeti and S. Santhanam, "Dispersion curves for Lamb wave propagation in prestressed plates using a semi-analytical finite element analysis," J. Acoust. Soc. Am. **143**, 829–840 (2018).
[20]Z. Yang, Z. Wu, J. Zhang, K. Liu, Y. Jiang, and K. Zhou, "Acoustoelastic guided wave propagation in axial stressed arbitrary cross-section," Smart Mater. Struct. **28**, 045013 (2019).
[21]P. Zuo, X. Yu, and Z. Fan, "Acoustoelastic guided waves in waveguides with arbitrary prestress," J. Sound Vib. **469**, 115113 (2020).
[22]N. Pei and L. J. Bond, "Higher order acoustoelastic Lamb wave propagation in stressed plates," J. Acoust. Soc. Am. **140**, 3834–3843 (2016).
[23]R. Murayama, "Non-contact stress measurement during tensile testing using an EMAT for SH0-plate wave and Lamb wave," J. Sensor Technol. **1**, 65–70 (2011).
[24]A. N. Norris, "Finite-amplitude wave in solids," in *Nonlinear Acoustics*, edited by M. F. Hamilton and D. T. Blackstock (Academic, San Diego, CA, 1998), pp. 263–277.
[25]Z. Abiza, M. Destrade, and R. W. Ogden, "Large acoustoelastic effect," Wave Motion **49**, 364–374 (2012).
[26]R. W. Ogden, "Elements of the theory of finite elasticity," in *Nonlinear Elasticity Theory and Applications*, edited by R. W. Ogden and Y. B. Fu (Cambridge University Press, Cambridge, UK, 2001), Chap. 1, pp. 1–57.
[27]S. Eldevik, "Measurement of non-linear acoustoelastic effect in steel using acoustic resonance," Ph.D. thesis, University of Bergen, Bergen, Norway, 2014.
[28]T. Hayashi, W. J. Song, and J. L. Rose, "Guided wave dispersion curves for a bar with an arbitrary cross-section, a rod and rail example," Ultrasonics **41**, 175–183 (2003).
[29]Z. A. B. Ahmad, "Numerical simulations of lamb waves in plates using a semi-analytical finite element method," Ph.D. thesis, University of Magdeburg, Magdeburg, Germany, 2011.
[30]I. Bartoli, A. Marzani, F. Lanza di Scalea, and E. Viol, "Modeling wave propagation in damped waveguides of arbitrary cross-section," J. Sound Vib. **295**, 685–707 (2006).
[31]J. L. Rose, *Ultrasonic Guided Waves in Solid Media* (Cambridge University Press, Cambridge, UK, 2014).
[32]J. R. Asay and A. H. Guenther, "Ultrasonic Studies of 1060 and 6061-T6 Aluminum," J. Appl. Phys. **38**, 4086–4088 (1967).
[33]A. Jäger, J. Hinrichs, G. Allevato, M. Sachsenweger, S. Kadel, D. Stasevich, W. Gebhard, G. Hubschen, T. Hahn-Jose, W. M. D. Wright, and M. Kupnik, "Non-contact ultrasound with optimum electronic steering angle to excite Lamb waves in thin metal sheets for mechanical stress measurements," in *Proceedings of the IEEE International Ultrasonics Symposium 2019*, Glasgow, UK (October 6–9, 2019), pp. 924–927.
[34]V. V. Mishakin, S. Dixon, and M. D. G. Potter, "The use of wide band ultrasonic signals to estimate the stress condition of materials," J. Appl. Phys. **39**, 4681–4687 (2006).
[35]R. B. Thompson, S. S. Lee, and J. F. Smith, "Angular dependence of ultrasonic wave propagation in a stressed, orthorhombic continuum: Theory and application to the measurement of stress and texture," J. Acoust. Soc. Am **80**, 921–931 (1986).